AIP | Review of Scientific Instruments

Multiobjective method for fitting pinhole image intensity profiles of implosion cores driven by a Pareto genetic algorithm

T. Nagayama, R. C. Mancini, L. A. Welser, S. Louis, I. E. Golovkin, R. Tommasini, J. A. Koch, N. Izumi, J. Delettrez, F. J. Marshall, S. P. Regan, V. Smalyuk, D. Haynes, and G. Kyrala

Citation: Review of Scientific Instruments **77**, 10F525 (2006); doi: 10.1063/1.2338314
View online: http://dx.doi.org/10.1063/1.2338314
View Table of Contents: http://scitation.aip.org/content/aip/journal/rsi/77/10?ver=pdfcov
Published by the AIP Publishing

Multiobjective method for fitting pinhole image intensity profiles of implosion cores driven by a Pareto genetic algorithm

T. Nagayama, R. C. Mancini, and L. A. Welser
Department of Physics, University of Nevada, Reno, Nevada 89557

S. Louis
Department of Computer Science, University of Nevada, Reno, Nevada 89557

I. E. Golovkin
Prism Computational Sciences, Madison, Wisconsin 53711

R. Tommasini, J. A. Koch, and N. Izumi
Lawrence Livermore National Laboratory, Livermore, California 94550

J. Delettrez, F. J. Marshall, S. P. Regan, and V. Smalyuk
Laboratory for Laser Energetics, University of Rochester, New York 14623

D. Haynes and G. Kyrala
Los Alamos National Laboratory, Los Alamos, New Mexico 87545

(Received 9 May 2006; presented on 11 May 2006; accepted 25 July 2006; published online 12 October 2006)

We discuss a method for the simultaneous and self-consistent fitting of a set of intensity or emissivity spatial profiles from several narrow-band x-ray pinhole images from argon-doped inertial confinement fusion implosion cores, and the space-integrated line spectrum. A Pareto genetic algorithm (PGA) combines the search and optimization capabilities of a single-objective genetic algorithm with the Pareto domination technique of multiobjective optimization. Further, the PGA search is followed up by a fine-tuning step based on a nonlinear least-squares-minimization procedure. The result is a robust search and reconstruction method that finds the optimal core spatial structure subject to multiple constraints. This method is independent of geometry inversions and could take advantage of not only optically thin but also optically thick image data. Results are shown for two combinations of three-objectives based on gated argon Heβ and Lyβ image data and the line spectrum. © *2006 American Institute of Physics.* [DOI: 10.1063/1.2338314]

I. INTRODUCTION

The extraction of the spatial distribution of temperature and density in an implosion core from the analysis of spectroscopic data is an important problem of direct- and indirect-drive inertial confinement fusion. One approach to attack this problem is based on a search and reconstruction in parameter space of the temperature and density spatial profiles that yield the best, simultaneous and self-consistent, fits to several pieces of data. Each piece of data to be fitted (i.e., approximated) represents an objective, and thus this search and reconstruction method is an example of multiobjective data analysis. In previous work, the use of genetic algorithms in single-objective spectroscopic data analysis, and two- and three-objective spectroscopic determination of implosion core spatial structure have been demonstrated using Pareto genetic algorithms (PGAs) to drive the search in parameter space.[1–3] The PGA combines the robustness and versatility of a single-objective genetic algorithm with the Pareto domination technique of multiobjective optimization. Here, we extend previous work on three-objective data analysis by (1) performing a more accurate calculation of the formation of the image intensity profile based on a numerical integration of the radiation transport equation, (2) showing that image plane intensity profiles can also be used as objectives, and (3) following up the PGA run with a nonlinear least-squares-minimization procedure for further improvement and refinement of the solution. The case of application is that of an argon-doped, deuterium-filled implosion core where a tracer amount of argon was added to the deuterium gas fill for diagnostic purposes. At the collapse of the implosion, bright argon line emission is recorded with a Multi-Monochromatic x-ray Imager (MMI) equipped with a pinhole array that records a large number of implosion core images, each one with a characteristic of a slightly different photon energy range.[4] Processing of these image data yields narrow-band x-ray pinhole images of the core characteristic of a photon energy range of the order of the broadening of the spectral line feature.[5]

II. MODEL

The atomic and radiation physics model employed to compute the intensity distribution of the pinhole core image considers the self-consistent solution of a set of collisional-radiative atomic kinetics rate equations and the radiation transport equation. Atomic processes include electron collisional excitation and deexcitation, electron collisional ioniza-

tion and recombination, spontaneous radiative decay and photoexcitation, stimulated emission, photoionization and radiative recombination, and autoionization and electron capture. The electron distribution function is assumed to be in equilibrium (i.e., Maxwellian) and detailed spectral line shapes account for Stark, Doppler, and natural broadening.[6] Once the argon atomic level populations have been determined, they are used to calculate the photon energy dependent emissivity and opacity distributions which are also dependent on the plasma electron density and temperature. The image intensity distribution is then computed via a numerical integration of the formal solution of the radiation transport equation along a discrete set of chords in the core; namely, the intensity at any point on the image is given by

$$I_\nu(y) = \int \varepsilon_\nu(x) e^{-\tau_\nu(x)} dx, \tag{1}$$

where y is the chord coordinate, x is an integration coordinate along the chord, ε_ν is the photon energy dependent emissivity, and τ_ν is the optical depth of a point of coordinate x along the chord. While the work in Refs. 1 and 3 assumed a slab geometry of physical thickness given by an average chord length, here we consider an axially symmetric core slice (or disk) and integrate Eq. (1) along a set of chords of different lengths in the disk. Hence, opacity effects are carefully taken into account both in the atomic level population calculation and in the transport of the radiation through the plasma source.

III. RESULTS

In order to illustrate the method, we apply it to data recorded in a series of indirect-drive shots performed at the OMEGA laser facility of the Laboratory for Laser Energetics at the University of Rochester. In these experiments plastic shells of 512 μm in diameter, wall thickness of 35 μm, and filled with 50 atm of deuterium and 0.1 atm of argon were driven by the radiation field created in a 2.5 mm long gold *Hohlraum* illuminated by 30 UV OMEGA beams each having an energy on target of 500 J.[3] The implosion was viewed through diagnostic holes drilled in the *Hohlraum* walls. The MMI instrument recorded x-ray gated narrow-band images in the photon energy range from 3000 to 5000 eV, which includes the argon Heβ ($1s^2\ ^1S - 1s3p\ ^1P$) and Lyβ ($1s\ ^2S - 3p\ ^2P$) lines and their associated Li- and He-like satellite transitions, respectively. This portion of the argon line spectrum was selected for analysis because it is sensitive to electron density and temperature through the density and temperature dependence of the level population kinetics and the density dependence of the Stark-broadened line shapes.[6]

The data for the analysis discussed here are taken from the central core slice recorded in indirect-drive OMEGA shot 36980,[3] and it is used both with the analysis method of Ref. 3 and the new PGA analysis discussed in this work. For a given set of input data, first, the PGA code is run to search in parameter space for a good approximation to the temperature and density spatial profiles that yield the best fits to the data. We emphasize that the PGA code starts the search with a random distribution of initial profiles and is thus unbiased.

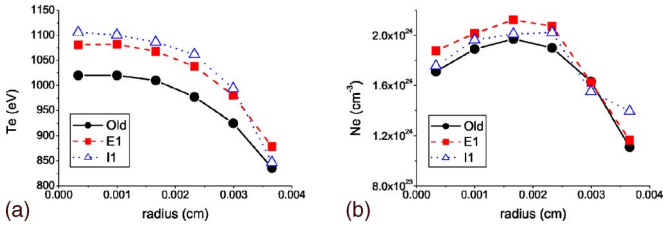

FIG. 1. (Color online) (a) Central core slice electron temperature spatial profiles based on three objectives: (1) Heβ and (2) Lyβ emissivities (or intensities) and (3) the space-integrated line spectrum. (E1): PGA results obtained using emissivities. (I1): PGA results obtained using intensities. PGA was run using optically thin radiation transport for computing the emergent intensity. (b) Central core slice electron density spatial profiles based on three objectives: (1) Heβ and (2) Lyβ emissivities or intensities and (3) the space-integrated line spectrum. (E1): PGA results obtained using emissivities. (I1): PGA results obtained using intensities. PGA was run using optically thin radiation transport for computing the emergent intensity.

Then, the best profiles found by the PGA are used to initialize a nonlinear least-squares-minimization procedure, based on the Levenberg-Marquardt method,[7] to further improve the quality of the fits. This two step procedure exploits the complementary characteristics of these algorithms. On the one hand, the PGA starts from an unbiased initialization and efficiently produces a good approximation to the optimal solution. A series of PGA runs where the only change is a different initial random seed is thus useful to check the uniqueness of the solution of the data fitting problem. On the other hand, the PGA result is also a very good initial seed for the nonlinear least-squares-minimization procedure which quickly converges to the optimal solution provided that it is well initialized. The PGA is not an efficient algorithm to perform this final convergence to the best solution. Hence, the combination of both algorithms represents an excellent strategy for objectively fitting data with a minimum number of assumptions.

The spatial grid uses a mesh of six zones for the radial r coordinate in the core slice (i.e., object space) and the y coordinate on the image plane. This is consistent with the spatial resolution expected for the MMI instrument which is about 7–10 μm;[4] no additional instrument effect is currently included. Figure 1 shows the electron temperature and density spatial distribution results obtained for three-objective data analysis where the objectives were the narrow-band (1) Heβ and (2) Lyβ emissivity or intensity spatial profiles, and the (3) space-integrated line spectrum covering the spectral range of these lines and their associated Li- and He-like satellite transitions (i.e., 3500–4000 eV photon energy range). The line spectrum was obtained from the same MMI data by computing a spatial integration over all core images recorded in the relevant spectral range.[3,4] Since the intensity of the image data is not absolutely calibrated, the line spectrum brings into the analysis an important constraint on the density through the density dependence of the Stark-broadened spectral line shapes. The experimental emissivity profiles were obtained from the image data intensity profiles via an Abel inversion.[8] We estimate the optical depths of these lines to be about 0.6 and 0.3, respectively. Since the Abel inversion assumes zero optical depth, these emissivity profiles ex-

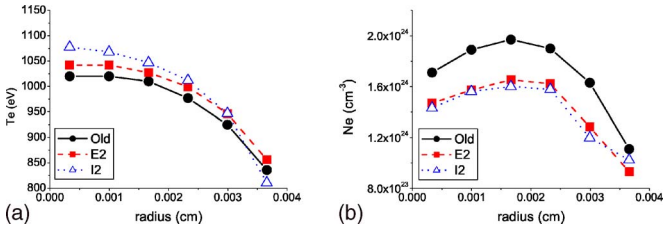

FIG. 2. (Color online) (a) Central core slice electron temperature spatial profiles based on three objectives: (1) Heβ and (2) Lyβ emissivities or intensities and (3) the space-integrated line spectrum. (E2): PGA results obtained using emissivites. (I2): PGA results obtained using intensities. PGA was run using full transport including absorption for computing the emergent intensity. (b) Central core slice electron density spatial profiles based on three-objectives: (1) Heβ and (2) Lyβ emissivities or intensities and (3) the space-integrated line spectrum. (E2): PGA results obtained using emissivities. (I2): PGA results obtained using intensities. PGA was run using full transport including absorption for computing the emergent intensity.

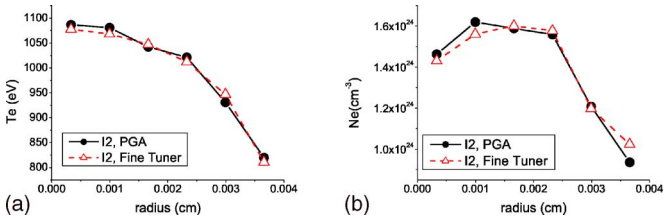

FIG. 3. (Color online) (a) Refinement of the PGA temperature spatial profile for case I2 of Fig. 2(a) performed by the (follow up) fine-tuner step. (b) Refinement of the PGA density spatial profile for case I2 of Fig. 2(b) performed by the (follow up) fine-tuner step.

tracted from data inversion represent an approximation to the actual emissivity. Two types of three-objective runs were performed with the new PGA code: using source emissivity profiles and line spectrum (labeled "E1" in Fig. 1) and using image intensity profiles and line spectrum (labeled "I1" in Fig. 1). In order to compare the new results with the result from the analysis code from Ref. 3 (labeled "old NGPA" in Figs. 1 and 2), we run the new PGA code in two different ways. One weak point of old npga is that it deals with the absorption and reemission effects in the calculation of the line spectrum in an approximate way: it uses an escape factor to adjust the total line intensities. Thus, for a first comparison with old NPGA, we run the new PGA code neglecting the absorption effect in the calculation of the space-integrated line spectrum. The results from these runs are shown in Fig. 1. We note that old NPGA method works only with emissivity profile data. Firstly, emissivity-objective results and intensity-objective results from the PGA runs compare well with each other indicating the feasibility of using either type of objective to drive the search in parameter space. Secondly, the comparison of density profiles obtained with old NPGA code and the current PGA method compare well both in shape and value. Since in both cases the broadening of the line shapes is dominated by the Stark broadening effect, the range of density values is the same. The temperature profiles though show a noticeable difference; this is a consequence of the escape factor correction used in the line spectrum calculation of old NPGA code. Not accounting for this effect requires a larger temperature to approximate the observed Lyβ and Heβ relative intensity.

Next, Fig. 2 displays the results obtained with the new PGA code now performing a full radiation transport calculation of the emergent intensity including the effects of absorption and reemission. Temperature profiles are now more comparable, since the opacity effect on the Lyβ to Heβ is now taken into account by both methods, but the densities of the PGA spatial profiles are now lower in value. The reason for this difference is that now the contribution to the total broadening of the line shapes due to the radiation transport leaves less room for the Stark broadening effect which then results in smaller values for the electron density. The results displayed in Figs. 1 and 2 account for both the optimization done by the PGA and the further refinement of the nonlinear least-squares minimization (i.e., "fine-tuner" step). To illustrate the level of improvement obtained by the fine-tuner step, Figs. 3(a) and 3(b) show for the case I2 of Fig. 2 the spatial profiles after the PGA run and after the PGA and fine-tuner runs. The effect of the fine tuner is then consistent with the idea of a refinement of the solution which is quickly accomplished by a few iterations of the least-squares-minimization algorithm. These data fitting results are encouraging and point to the fact of the efficiency and robustness of the whole procedure. Further work is in progress to extend this method to more simultaneous objectives and to include an estimation of the error bars.

ACKNOWLEDGMENTS

This work is supported by DOE-NLUF Grant DE-FG52-2005NA26012 and LLNL under Contract W-7405-Eng-48.

[1] I. Golovkin *et al.*, Phys. Rev. Lett. **88**, 045002 (2002).
[2] I. E. Golovkin, R. C. Mancini, S. J. Louis, R. W. Lee, and L. Klein, J. Quant. Spectrosc. Radiat. Transf. **75**, 625 (2002).
[3] L. A. Welser *et al.*, J. Quant. Spectrosc. Radiat. Transf. **99**, 649 (2006).
[4] J. A. Koch, T. W. Barbee, Jr., N. Izumi, R. Tommasini, R. C. Mancini, L. A. Welser, and F. J. Marshall, Rev. Sci. Instrum. **76**, 073708 (2005).
[5] L. A. Welser *et al.*, Rev. Sci. Instrum. **74**, 1951 (2003).
[6] I. Golovkin and R. C. Mancini, J. Quant. Spectrosc. Radiat. Transf. **65**, 273 (2000).
[7] W. H. Press, B. P. Flannery, S. A. Teukolsky, and W. T. Vetterling, *Numerical Recipes in C* (Cambridge University Press, Cambridge, 1997).
[8] K. Bockasten, J. Opt. Soc. Am. **51**, 943 (1961).